Minerals Engineering 63 (2014) 139–148

Contents lists available at ScienceDirect

Minerals Engineering

journal homepage: www.elsevier.com/locate/mineng

Numerical simulations of comminution slurries over complex topographies: Putting together CFD and pipeline integrity

Tomás Trewhela [a,*], Christian Ihle [b,c], Aldo Tamburrino [d,c]

[a] Master Program on Water Resources and Environment, Department of Civil Engineering, Universidad de Chile, Blanco Encalada 2002 3rd Floor, Santiago, Chile
[b] Department of Mining Engineering, Universidad de Chile, Tupper 2069, 8370451 Santiago, Chile
[c] Advanced Mining Technology Center, Universidad de Chile, Tupper 2007 3rd Floor, 8370451 Santiago, Chile
[d] Department of Civil Engineering, Universidad de Chile, Blanco Encalada 2002 3rd Floor, 8370449 Santiago, Chile

ARTICLE INFO

Article history:
Received 11 September 2013
Revised 6 March 2014
Accepted 10 March 2014
Available online 31 March 2014

Keywords:
Computational fluid dynamics
Environmental
Simulations

ABSTRACT

The use of computational fluid dynamics gives new and interesting insights for risk analysis of cross-country ore hydraulic transport operations. In particular, they offer the possibility to predict, with reasonable accuracy, the progression and final condition of spills driven by pipeline leaks at selected locations, at a relatively modest computational cost. In this work, a depth-averaged, two-dimensional numerical model is used to simulate an ore concentrate pipeline rupture and subsequent spill, reproduced as a constant flow condition at the leak point. Although the model is well suited to solve the governing flow equations on arbitrary topographies by means of digital elevation models, two specific locations featuring relatively mild and steep slopes, are analysed with regard to their implications on the potential requirements for emergency team response. Results, obtained using different slurry rheologies, are compared with those obtained using a simpler, common flow resistance model derived for water flowing over rough surfaces.

© 2014 Elsevier Ltd. All rights reserved.

1. Introduction

Computational fluid dynamics (CFD) is often used for different flow problems and phenomena whose behaviour and prediction is not easily described with simple conceptual models (Xia and Sun, 2002). The phenomenology and modelling of ore concentrate hydraulic transport operations is not the exception. Sudden ruptures affecting the integrity of pipeline systems transporting slurries such as concentrates and tailings involve sudden discharges as well, with a subsequent flow over the surrounding location at which the leak started. The spreading of such kind of slurry over cross-country locations could possibly reach towns, environmentally protected areas or cultivated lands, thus affecting sources of water and food (Minas, 2010). The use of CFD therefore opens a door for the prediction and the identification of specific points along the pipeline route that should be treated as special or sensitive locations. The intent of planning activities to maximize the integrity of a cross-country pipeline offers a permanent challenge to the capacity of reaction and placement of response teams and resources related to mitigation measures when a leak incident occurs.

Spills due to pipeline leaks or ruptures can be easily modelled as a certain fluid volume being expelled with high velocities at a specific location. From this time on, the spill starts flowing over the surface and might become quite complex depending on the local topography characteristics. In order to describe these flows, a wealth of numerical schemes is available in order to solve the equations of mass and momentum conservation (Jia and Wang, 1999; Biscarini et al., 2010). In particular, two-dimensional models, which are in general able to describe with reasonable accuracy the spreading characteristics of leak flows in natural terrains, offer an ideal combination of detail and computational cost. In this paper, GeoClaw, an open-source, two dimensional numerical code oriented to the study of geophysical flows, has been conveniently adapted to model the aforementioned special kind of fluid flows, not only regarding how the run-out evolves over the topography and time, but also describing a more realistic discharge of a slurry, described as an equivalent homogeneous fluid with particular rheological characteristics.

GeoClaw, as other two dimensional models, solves the long-wave, vertically averaged Saint Venant Eqs. (1a)–(1c) with bottom and surface shear stress boundary conditions (Berger et al., 2011).

* Corresponding author. Tel.: +56 996403201.
E-mail address: ttrewhel@ing.uchile.cl (T. Trewhela).

http://dx.doi.org/10.1016/j.mineng.2014.03.005
0892-6875/© 2014 Elsevier Ltd. All rights reserved.

Saint Venant equations as solved numerically are expressed under its weak form as:

$$\frac{\partial H}{\partial t}+\frac{\partial (UH)}{\partial x}+\frac{\partial (VH)}{\partial y}=0 \tag{1a}$$

$$\frac{\partial (UH)}{\partial t}+\frac{\partial}{\partial x}\left(\beta_{xx}U^2H+\frac{gH^2}{2}\right)+\frac{\partial (\beta_{xy}UVH)}{\partial y} = -gH\frac{\partial z_b}{\partial x}+\frac{1}{\rho_m}(\tau_{xz}|_{z_b+H}-\tau_{xz}|_{z_b}) \tag{1b}$$

$$\frac{\partial (VH)}{\partial t}+\frac{\partial (\beta_{yx}UVH)}{\partial x}+\frac{\partial}{\partial y}\left(\frac{gH^2}{2}+\beta_{yy}V^2H\right) = -gH\frac{\partial z_b}{\partial y}+\frac{1}{\rho_m}(\tau_{yz}|_{z_b+H}-\tau_{yz}|_{z_b}), \tag{1c}$$

where H is the flow depth, U and V are the velocities in the x and y directions, respectively. The term τ_{iz} denotes the shear stresses evaluated at $(z_b + H)$ and z_b for the ith direction, respectively. Since z_b is an arbitrary datum referred to the altitude as a coordinate, the last two terms in Eqs. (1a) and (1b) are the shear stresses at the surface and the bottom respectively for each direction. To simplify the notation, the mean velocity in the ith direction is written hereafter as U_i. The shape factors β_{ij} are the Boussinesq coefficients whose appearance is a consequence of using the vertical mean velocities in the momentum equations, defined as:

$$\int_{z_b}^{z_b+H} u_i u_j dz = \beta_{ij}U_iU_jH \tag{2}$$

Several considerations are taken into account in order to simplify the solution carried out by the numerical solver. The Boussinesq coefficients values are considered to be unitary and the shear stresses at the surface are neglected as a result of no further external stresses applied to the flow.

The modifications to this model include an implementation of a constant discharge flow rate and the inclusion of rheology as a sensitive parameter, which is given as an input. The ore concentrate for hydraulic transportation is composed primarily by a mixture of ore at a given concentration with water. This comminution slurry behaves differently than water and its rheology is similar to that of a Bingham plastic, and for slender fluid flows is given by Abulnaga (2002); Chhabra and Richardson (2008):

$$\eta\dot{\gamma}=\begin{cases}0 & \tau\leqslant\tau_y\\ \tau-\tau_y & \tau>\tau_y\end{cases} \tag{3}$$

with η as the plastic viscosity, τ the fluid shear stress, τ_y the yield stress and $\dot{\gamma}$ the shear rate. This definition establishes dissimilarities from the well-known water behaviour. In this paper, both rheological descriptions, *viz* Newtonian-water – and non-Newtonian-slurry–, represented by a Bingham plastic, will be considered for the modelling of the fluid. The usage of the Bingham plastic model is well accepted (Bird et al., 1983) and widely used by the mining industry supported on the low variety of grain-size species, with the presence of small sized material. Small sizes favours homogenous mixture, a strong requirement for the usage of rheological models which settles proper conditions for shear stress calculations (Ihle and Tamburrino, 2012b). For the present work the Bingham plastic model will be considered suitable for the fluid modelling.

Most of the available two-dimensional models use water as the fluid. To ease a comparison between water and non-Newtonian fluid-based model outcomes-based on the same flow equations –, both of them will be considered herein. Saint Venant equations require two shear stress terms, included as bottom and surface boundary conditions for the vertical fluid column. The last terms in Eqs. (1b) and (1c), corresponding to the bed friction terms, are commonly modelled with a constant, Manning coefficient. The Manning coefficient formulation for the bed friction term is a widely used expression in two dimensional flow models; nevertheless, it is valid only for water flowing in the turbulent regime over a hydrodynamically rough bed, a condition that is not always accurate for the unconfined or weakly confined flows such as those referred in this study. The surface friction terms, which commonly reflect the presence of wind, will be neglected herein.

An alternative formulation for the bed friction terms based on the Darcy friction factor is made. The latter is defined as $f_i = 8\tau_{iz}|_{z=z_b}/(\rho_m U_i|U_i|)$, where ρ_m is the mixture density. This implies the existence of a dependence of the flow regime as well as of the hydrodynamic condition of the bed. The bed friction term is usually related to a hydraulic gradient, J_i, as:

$$\tau_{iz}|_{z=z_b}=\rho_m gHJ_i, \tag{4}$$

The mixture density, ρ_m, may be expressed as:

$$\rho_m=(1-\phi)\rho+\phi\rho_s, \tag{5}$$

where ϕ is the volume concentration of solids, ρ_s is the solids density and ρ is the water density. This allows the inclusion of the concentration and the rheology in the model, and will yield a local friction factor for each simulation resulting on the coupling of fluid properties and flow resistance in this time- and space-dependent problem. This provides a point of comparison with a global Manning coefficient defined solely in terms of the terrain characteristics. It is noted that both the Manning and Darcy formulations are related to the hydraulic gradient.

The modelling is generated considering a matrix of probable events combining two distinct topographic scenarios, three flow rates and four bed friction formulations, namely (i) water with a global Manning coefficient, (ii) water using a Darcy coefficient covering the various possible flow regimes and bed behaviours, (iii) an iron concentrate flow – with the slurry modelled as a Bingham plastic – with $\phi = 0.25$ and (iv) an iron concentrate flow, this time with $\phi = 0.4$. It is noted that (iii) and (iv) use a rheology-dependent Darcy coefficient and a value of ρ_s equal to 5200 kg/m^3.

In this paper, the results of the computations using the four bed friction formulations referred above is presented and discussed. The analysis also extends to the model features and its convergence. Finally, the discussion is focused on the implications of using such different friction and rheology approaches and the influence of CFD in pipeline rupture problems and decision-making facing leak possible leak events.

2. Model description

In the present work, GeoClaw, an open source code used for geophysical flows, will be utilised. With a low memory usage, an interface programmed in PYTHON and the model written in FORTRAN, it represents an overall convenient computational option. The model itself includes a solution for the wet–dry cell problem, a mesh refinement tool that optimizes the memory usage improving computation times and providing a stable operation with robust methods, among other features (George and Le Veque, 2006, 2008). In this study, both the set of features and the open source scheme blends well with code adaptions. GeoClaw uses a finite volume scheme, which ensures mass conservation. The numerical solution of the Saint Venant equation often encounters problems in the advection term treatment (Toro, 1997). In order to solve the advective terms (the second and third terms at the left of Eqs. (1b) and (1c)), Riemann solvers must be implemented. The Riemann problem consists of a wave-propagation problem with two boundary conditions that is considered constant piecewise,

for which, Godunov in 1959 introduces an exact solution. This has a variety of numeric implementations, most of them based on the Godunov advection scheme (Toro, 1997). GeoClaw has a simple, yet optimized solution for the Riemann problem (Toro, 1997), allowing the user the possibility to improve the order of the solution as described by George (2008). The solution presented by GeoClaw, based on Godunov, linearizes the non-linear terms (second and third terms in Eqs. (1b) and (1c)).

A common feature of all the computational approaches solving the Saint Venant equations for two-dimensional flows is the global Manning coefficient-based modelling of the bed friction (Aldrighetti and Zanolli, 2005; Brufau and Garcia-Navarro, 2000). GeoClaw is not the exception, and the treatment of the bottom friction terms is local, albeit with a user-defined global Manning coefficient, with the implications discussed above.

The first adaption made to the software was oriented to the implementation of a constant discharge at an arbitrary location (cell) or area of flooding. Thus, it is possible to input values for height and flow rates in both directions at a given location or area. The resulting source flow conditions are defined as:

$$\begin{aligned} H(x^*, y^*) &= H^* \\ q_x(x^*, y^*) &= q_x^* \\ q_y(x^*, y^*) &= q_y^*, \end{aligned} \tag{6}$$

where H^* is the flow height over a point or interval of discharge (x^*, y^*) and q_i are the flow rates per width in the ith direction over the same point or interval, imposed by the discharge curve. Then, the discharge curve is described by the vectorial relation $Q(x^*, y^*) = (H^*, q_x^*, q_y^*)$.

Further modifications have been done in the present implementation regarding the bed friction terms. The Manning formulation to determine the hydraulic gradient by means of a roughness coefficient, as originally implemented, is given by:

$$J_i = \frac{U_i|U_i|n^2}{H^{4/3}}, \tag{7}$$

where J_i is the hydraulic gradient in the ith direction, H is the flow depth, U_i is the mean velocity in the ith direction and n is the Manning coefficient. On the other hand, the hydraulic gradient for a Bingham plastic and Newtonian fluid is related to a Darcy friction coefficient, f, through the Darcy–Weisbach equation in the ith direction as:

$$J_i = \frac{f_i}{4H}\frac{U_i|U_i|}{2g}. \tag{8}$$

In order to estimate the values of the coefficients f_i, it is necessary to identify the flow regime, which may be either laminar or turbulent. This is done by means of a Reynolds number, defined as:

$$Re_{B\mu_i} = \frac{4\rho_{mU_iH}}{\eta\left(1+\frac{2}{3}B_i\right)}, \tag{9}$$

which is defined in terms of the Bingham number, B_i:

$$B_i = \frac{\tau_y H}{\eta U_i} = HeRe_{B_i}, \tag{10}$$

where He is the Hedström number, given by:

$$He = \frac{16\tau_y H^2 \rho_m}{\eta^2}. \tag{11}$$

Although the condition at which the flow of a non-Newtonian fluid departs from its laminar behaviour and become fully turbulent is still a matter of research, a modified Reynolds number is commonly defined to establish the limits between the different flow regimes (Chhabra and Richardson, 2008). Following Eshtiaghi et al. (2012), the laminar regime is given by $Re_{B\mu} < 2100$, and the turbulent regime by $Re_{B\mu} > 4000$. Intermediate values of $Re_{B\mu}$ correspond to the laminar-turbulent transitional regime.

To compute the Darcy friction coefficient for Bingham plastic flows, another Reynolds number is also defined:

$$Re_{B_i} = \frac{4\rho_m U_i H}{\eta} = Re_{B\mu_i}\left(1+\frac{2}{3}B_i\right). \tag{12}$$

The Darcy friction factor for laminar flow of a Bingham plastic, $Re_{B\mu} < 2100$, is calculated from the Buckingham equation (Buckingham, 1921) , which in dimensionless form is given by Darby (2001):

$$f_i = \frac{16}{Re_B}\left(1+\frac{He}{6Re_{B_i}}-\frac{He^4}{3f_i^3 Re_{B_i}^7}\right), \tag{13}$$

where an analytical solution has been recently found, including asymptotic expressions for small and large values of the Bingham number (Ihle and Tamburrino, 2012a). Eq. (13) is independent of the topography roughness, as expected for a laminar flow (White, 2003). In contrast, for turbulent flow, and to be able to hydrodynamically classify the bed, is necessary to introduce a Reynolds number based on the bottom roughness, k_s, as $Re_k = \rho u_* k_s/\mu$, where u_* is the shear velocity (Nikuradse, 1950; Keulegan, 1938). After some manipulation, it can be written as:

$$Re_{k_i} = \frac{k_s}{8H}\sqrt{\frac{f_i}{2}}Re_{B_i}. \tag{14}$$

Among the smorgasbord of relationships for the friction factor of turbulent flows of non-Newtonian fluids (see references in, for example, Chhabra and Richardson, 2008; Skelland, 1967, etc.), a set of expressions based on those obtained for Newtonian fluids with a suitable Reynolds number will be used in this paper (Chhabra and Richardson, 2008; Skelland, 1967; Wasp et al., 1977). In particular, the pipe diameter is replaced by four times the hydraulic radius or the flow depth (Keulegan, 1938). Thus, for turbulent flow over a hydrodynamically smooth bed ($Re_{B\mu} > 4000$ and $Re_{k_i} < 5$), the friction factor is computed as:

$$\frac{1}{\sqrt{f_i}} = 2.27\log(Re_{B_i}\sqrt{f_i}) - 1.451 + 2.25\log(1-\alpha_i), \tag{15}$$

where α_i is the yield-to-bottom stress ratio:

$$\alpha_i = \frac{\tau_y}{\rho_m g H J_i}. \tag{16}$$

The expression (15) is similar to that proposed by Torrance (1963) and Thomas and Wilson (1987). Under the condition of $Re_{B\mu_i} > 4000$ and $Re_{k_i} > 60$ the flow is classified as turbulent over a hydrodynamically rough bed, and the friction factor is given by:

$$\frac{1}{\sqrt{f_i}} = 2\log\left(\frac{2H}{k_s}\right) + 1.68. \tag{17}$$

For the transition between hydrodynamically smooth and rough wall ($Re_{B\mu_i} > 4000$ and $5 < Re_{k_i} < 60$), the transitional friction factor is computed using the following expression (Faddick, 1985):

$$f_i = \frac{f_{water-rough_i}}{f_{water-smooth_i}} f_{Bingham-smooth}, \tag{18}$$

here, the "water" subscript points to the requirement of calculations using friction factor expressions for water but evaluated using the Reynolds number for Bingham plastics (Re_{B_i}), and the term $f_{Bingham-smooth}$ stands for the estimation of a f coefficient using Eq. (15). The expression for the calculation of $f_{water-smooth}$ is the following (White, 2003):

$$\frac{1}{\sqrt{f_{water-smooth_i}}} = -2\log\left(\frac{2.51}{Re_{B_i}\sqrt{f_{water-smooth_i}}}\right), \tag{19}$$

and for $f_{water-rough}$, Eq. (17) is used since it resembles the similar relation for water (White, 2003).

The transition between laminar and turbulent flows is covered by a metric using the friction factors for each of the regimes (Darby, 2001):

$$f_i = \left(f^{m_i}_{Bingham-laminar_i} + f^{m_i}_{Bingham-turbulent_i}\right)^{1/m_i}, \tag{20}$$

where m_i is an empirical parameter, expressed as:

$$m_i = 1.7 + 40000/Re_{B_i}. \tag{21}$$

In Eq. (20), the $f_{Bingham-laminar}$ term requires the estimation of a friction factor, as if the flow was in laminar regime, using Eq. (13) and analogously, $f_{Bingham-turbulent}$ requires calculations, as if the flow was in turbulent regime, using Eqs. 15, 17, 18, depending on the hydrodynamic wall classification.

The incorporation of the previous equations in the modified code has allowed to expand the capabilities of the original software to any flow regime for either Newtonian or Bingham plastic fluids.

Eqs. (1a)–(1c) may be written in dimensionless form as:

$$\frac{\partial \bar{h}}{\partial t} + \frac{\partial(\bar{u}\bar{h})}{\partial x} + \frac{V^* L_x}{U^* L_y}\frac{\partial(\bar{v}\bar{h})}{\partial y} = 0 \tag{22a}$$

$$Fr_x^2\left(\frac{\partial(\bar{u}\bar{h})}{\partial t} + \frac{\partial(\beta_{xx}\bar{u}^2\bar{h})}{\partial x} + \left(\frac{V^* L_x}{U^* L_y}\right)\frac{\partial(\beta_{xy}\bar{u}\bar{v}\bar{h})}{\partial y}\right) = -\bar{h}\frac{\partial(\bar{z}_b + \bar{h})}{\partial x} - Fr_x^2\left(\frac{L_x}{H^*}\frac{f_x\bar{u}|\bar{u}|}{8}\right) \tag{22b}$$

$$Fr_y^2\left(\frac{\partial(\bar{v}\bar{h})}{\partial t} + \left(\frac{U^* L_y}{V^* L_x}\right)\frac{\partial(\beta_{yx}\bar{u}\bar{v}\bar{h})}{\partial x} + \frac{\partial(\beta_{yy}\bar{v}^2\bar{h})}{\partial y}\right) = -\bar{h}\frac{\partial(\bar{z}_b + \bar{h})}{\partial y} - Fr_y^2\left(\frac{L_y}{H^*}\frac{f_y\bar{v}|\bar{v}|}{8}\right), \tag{22c}$$

where $\bar{u}$ and $\bar{v}$ are the dimensionless vertically-averaged velocities for directions x and y respectively, $\bar{h}$ is the dimensionless flow height, $\bar{z}_b$ is a dimensionless datum, L_i are characteristic lengths for the ith direction. A Froude number for the flow in the ith direction, Fr_i, appears naturally from the scaling, and it is defined as:

$$Fr_i^2 = \frac{U_i^{*2}}{gH^*}, \tag{23}$$

where U_i^* is a velocity scale in the ith direction and H^* is a height scale both of them characteristic to the problem. Other, two dimensionless numbers appear (δ and ε_i), that take into account aspect ratio relations of the phenomenon. They are defined as.

$$\delta \equiv \frac{V^* L_x}{U^* L_y} \tag{24}$$

and

$$\varepsilon_i \equiv \left(\frac{L_i}{\bar{h}}\right)^{-1}. \tag{25}$$

It is noted that, given the present scaling, the terms including derivatives are on the order of the unity. The same applies for the terms $\frac{L_x}{H^*}\frac{f_x\bar{u}|\bar{u}|}{8}$ and $\frac{L_y}{H^*}\frac{f_y\bar{v}|\bar{v}|}{8}$ in the second term of the right hand side of (22a) and (22b). The definitions introduced in (24) and (25) indicate which scales are dominant in the dynamics of the flow, as will be shown hereafter.

3. Case description

The following cases are considered in the present paper: two different flow rates, two topographic locations in which the discharge is made, and two formulations for the bed friction stresses where, in the case of the Darcy formulation, 3 different slurry concentrations are considered. The flow rates are 10% and 50% of a maximum discharge value (1200 m^3/h), a choice made to resemble the order of magnitude of tonnages of some iron ore concentrate pipelines. Although the present model is unable to compute possible jets induced at the leak points due to incipient small cross-sectional bores at the pipe, the highly abrasive characteristic of the slurry would plausibly cause a larger hole soon after, thus inducing a lower discharge velocity. Thus, for the sake of obtaining illustrative figures, the flow velocity at the source has been set herein to 3 m/s. Scenarios for the discharge points are taken from real topography locations and they are arbitrary selected to reproduce both a mild and a steep slope. On the friction factor considerations, a Manning-based formulation for water (originally supported by GeoClaw) is opposed to Darcy's formulation evaluated with three different fluids: water and two Bingham plastics, the latter with volumetric concentrations of 25% and 40%, respectively.

The Manning-based formulation of the bottom shear stress for water flow employs a user-defined value for the Manning coefficient. An additional step is taken, for a consistent determination of the coefficient, as the Strickler formula for bed particles is used to estimate the coefficient (Limerinos, 1970).

$$n = 0.038 d_s^{1/6} \tag{26}$$

where d_s is a representative diameter of the bed particles, assumed as 10 cm. To allow for a side-by-side comparison, k_s, the roughness height used in (14) and (17), has been set to 10 cm, so that both formulations, Manning and Darcy, have an equivalent roughness.

The Darcy formulation is suitable to incorporate both Newtonian rheology for water and those of hyperconcentrated slurries such as Bingham plastic-type ore concentrates. In our example, Krieger-type expression is used to relate the slurry plastic viscosity with its concentration (Mewis and Wagner, 2011, and references therein):

$$\frac{\eta}{\mu} = \left(1 - \frac{\phi}{\phi_m}\right)^{-X_\eta}. \tag{27}$$

Here, the parameters $X_\eta = 2$ and $\phi_m = 0.47$, describing the characteristics of some ore concentrates (Ihle, 2013) have been considered. The yield stress has been modelled similarly (Heymann et al., 2002).

$$\tau_y = \hat{\tau}(\phi_m - \phi)^{-X_\tau}, \tag{28}$$

where $\hat{\tau}$ is a constant for the yield stress relation with a value of 0.038 Pa (Ihle, 2013) and, analogously to the plastic viscosity model, $X_\tau = 2$ is assumed herein.

The simulation for each combination comprises a 2-h slurry run-out. The output consists of values for length and height at points for which at a certain time the spreading is maximum in the main direction of the flow. In each simulation, measurements are taken 5, 20, 40, 60, 80, 100 and 120 min after the spill starts, and for each time the location of the farthest point is determined and saved for subsequent evaluation of its height.

As an example of a reference on required reaction times in front of a spill, two potentially important points in the path of the spill are referenced. Such points are arbitrarily located at 159 m from the discharge point in the mild slope scenario and at 815 m from the discharge point in the steep slope scenario.

4. Convergence tests and grid size determination

Results were first validated by means of a convergence test, for different numbers of grid elements. Simulations for both scenarios were performed to relate convergence with spatial resolution. The grid size was chosen based on these results and the test was performed using 6400, 57600, 102400, 160000 and 230400 grid elements. The corresponding results are shown in Fig. 1 for the two referred topographic scenarios. The comparison between the outputs corresponding to the different cases has been made *via* the maximum length for each simulation as defined above. For all the cases, the same formulation for the flow resistance and the fluid has been considered, i.e., Darcy and a non-Newtonian rheology, and a 600 m^3/h spill flow rate.

According to Fig. 1, the convergence seems acceptable for a model of such characteristics and complexity. It is noted that using grid elements in excess of 1,00,000 does not seem to yield great differences in the output and, on the other hand, the available computational resources limit the maximum number of grid elements that can be considered. Additionally, there is a significant limitation on the topographic data side; in particular, to the knowledge of the authors there are no available digital elevation models able to provide topographic data with resolutions better than one metre. Therefore, even fixing the total grid number to hundreds of thousands will not span an area smaller than 1 square kilometer. A trade-off between the spatial resolution of the available elevation data and the computational cost has been obtained using a 160000-element grid, of 5.56×5.56 m^2. With this setting, using a 3.4 Ghz processor with 7.9GB RAM, each case took about 40 min CPU time.

5. Results

The spreading of the spill is shown in Figs. 2–5. Figs. 2–4 show the run-outs for the mild slope topographic scenarios for the same flow rate (50% of maximum flow rate, i.e., 600 m^3/h), with the two different formulations of the bottom shear stress and the different slurry concentrations considered. Fig. 5 shows the flow run-out for the steep slope scenario for the same flow rate than Figs. 2–4, but only including a comparison between the Manning-based and the Darcy-based formulation for the water flow. The reason why there is only one comparison for the steep slope scenario is due to the fact that almost identical results were found in this case.

Fig. 2 compares the results of the flow run-out using the Manning and Darcy coefficient (first and second row, respectively), where the latter formulation is evaluated for water.

As an extension of the comparison exposed above for the same mild slope scenario, Fig. 3 shows two spills formulated under the Darcy formulation, but each of them representing different solids concentrations; the top row is for water (Newtonian or, equivalently in this context, $\phi = 0$) and bottom row is for $\phi = 0.25$. Fig. 4 shows two run-out scenarios, also formulated under the Darcy coefficient hypothesis; both of them correspond to Bingham slurries, with top and bottom rows standing for volumetric concentrations $\phi = 0.25$ and $\phi = 0.4$, respectively.

Fig. 6 presents the maximum lengths of the run-out for both topographic scenarios, achieved with discharge flows equal to 10%, and 50% of the maximum flow rate (each of them representing a column of Fig. 6). These lengths follow the principal direction of the flow and therefore do not necessarily correspond to straight lines or the same path for different slurry and/or discharge conditions.

For each of the two topographies considered, an arbitrary checkpoint has been selected and marked with squares (Figs. 2–5). These points could represent a river, a lake, a populated area or a natural reserve for which a response team should possibly need to act to avoid flooding. Fig. 7 simulates, for both topographies, the height of the spreading as a function of time at the checkpoint for each of the scenarios. The flow rate is 50% of the maximum discharge (600 m^3/h), where the impact of the choice of the formulation and the concentration is clear.

6. Discussion

Compared to the Darcy coefficient formulation, the approach using the Manning coefficient tends to overestimate the run-out lengths, regardless the solids concentration in consideration. The explanation for such overestimation resides in the assumptions Manning's formula. The Manning coefficient is valid for turbulent flow of water over a hydrodynamically rough bottom, a condition that the present flows does not always satisfy. In particular, due to the slender condition of the spreading of these mudflows, the laminar, as well as the laminar-turbulent transitional regime, may be found. On the other hand, even in the turbulent regime, a condition of a hydrodynamically smooth bed may be found, thus creating a coupling between inertial and viscous forces through

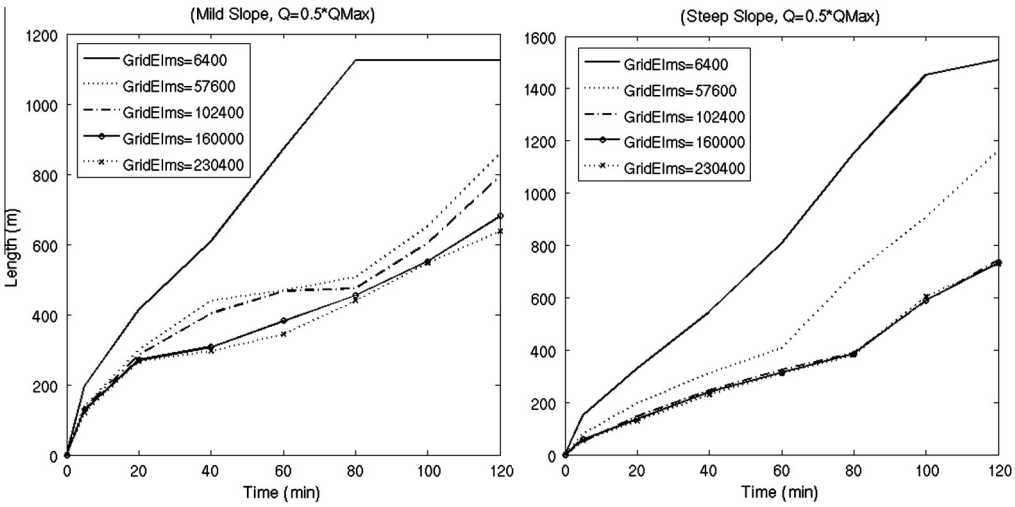

Fig. 1. Convergence test using 6400, 57600, 102400, 160000 and 230400 grid nodes. The left and right panels represent the mild and steep slope, respectively. The variable analysed is the run-out length for a spill of 600 m^3/h with a Darcy formulation using a Bingham plastic ($\phi = 0.4$) fluid.

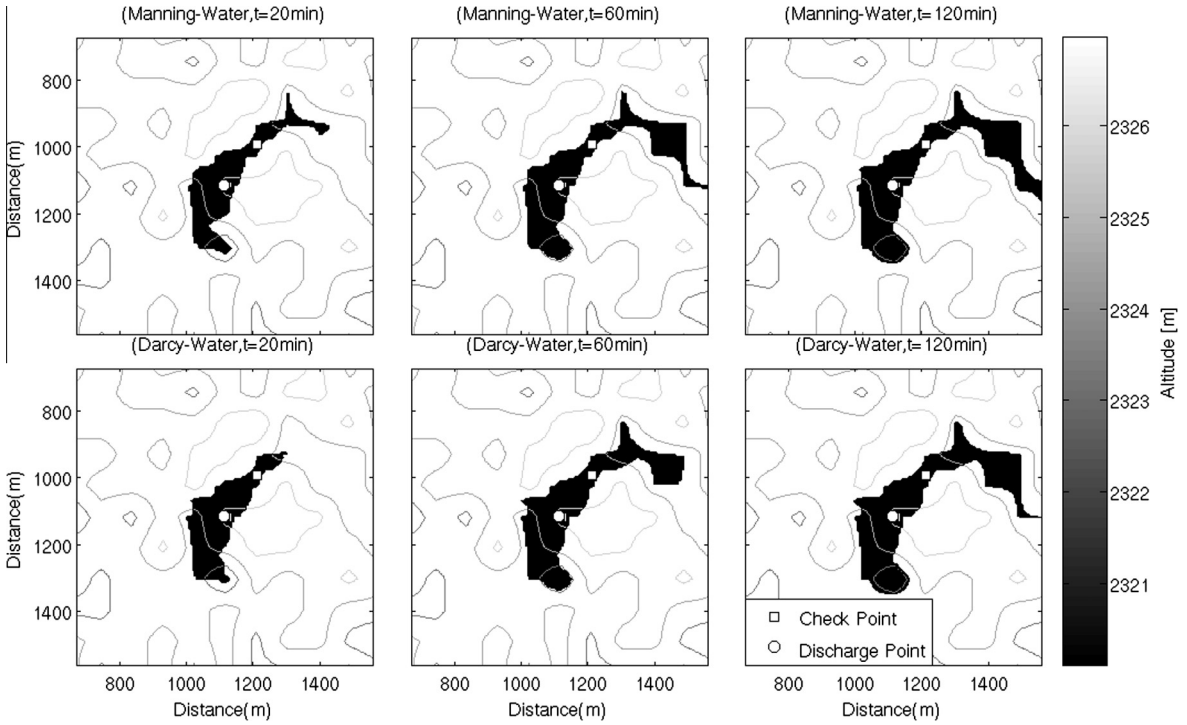

Fig. 2. Water run-out in the mild slope scenario and a 600 m^3/h discharge flow. The first and second rows show the simulation results using the Manning and Darcy coefficient formulations, respectively. See Section 6 for a reference to the checkpoint.

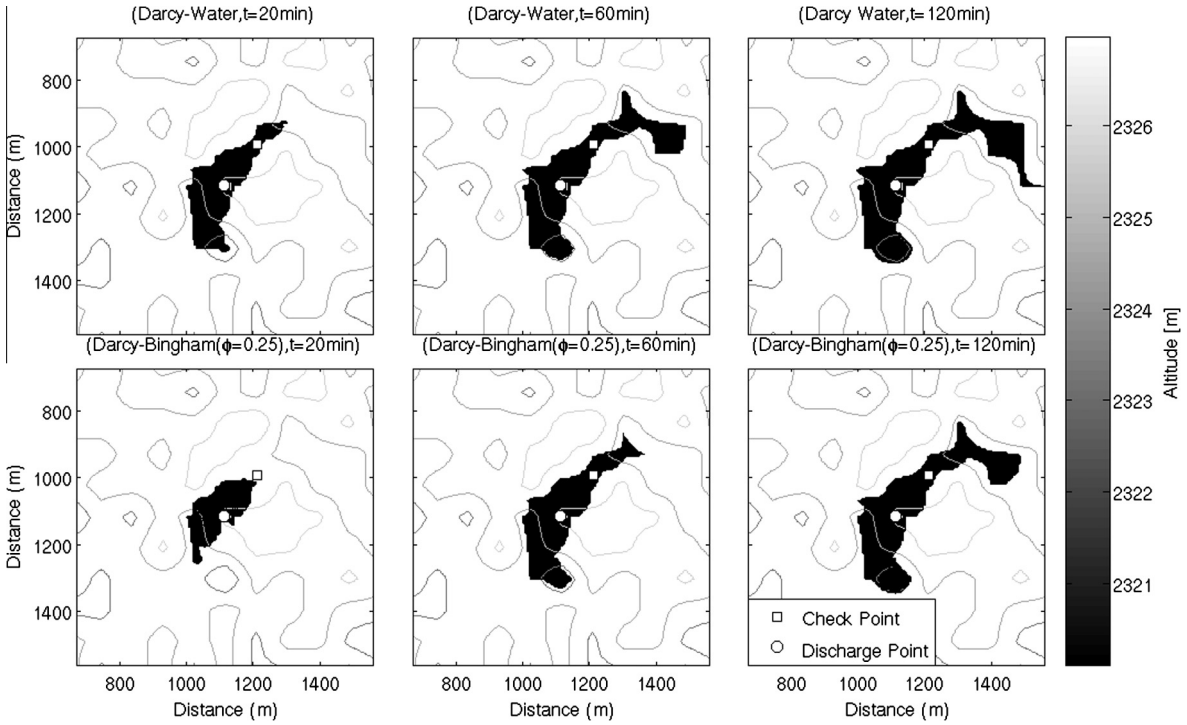

Fig. 3. Water and slurry run-out in the mild slope scenario using the Darcy coefficient formulation and a discharge flow of 600 m^3/h. First row: water. Second row: Bingham slurry ($\phi = 0.25$).

the Reynolds number dependence. A figure of the potential for significant differences between both modelling approaches may be observed from (6) and (7), whence $n \sim f^{1/2}H^{1/6}$, and also $J \sim V^2 f/H$, i.e., there is a dependency of the Manning coefficient n with the Reynolds number and the relative roughness, k_s/H. In general, the well-known decrease of f (and n) with the mean velocity is not entirely modelled in GeoClaw, a fact that is not considered in the original implementation of GeoClaw. The consistent run-out

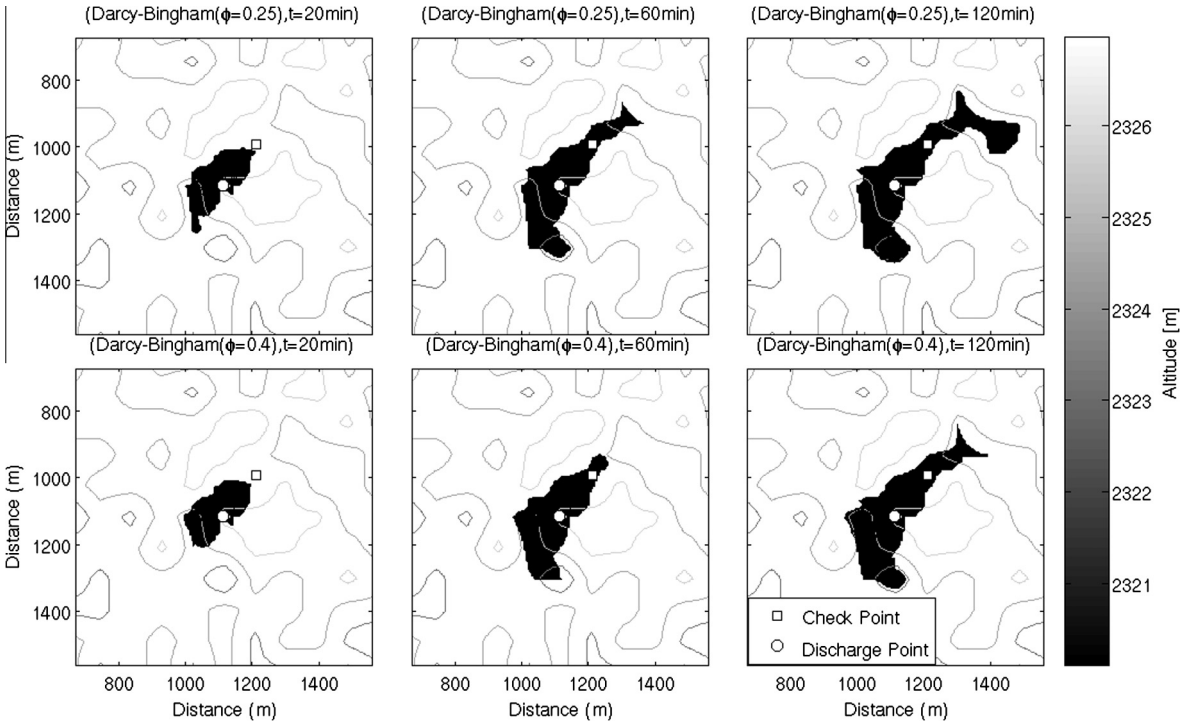

Fig. 4. Slurry run-out in the mild slope scenario for a 600 m^3/h discharge flow. The first and second rows represent the cases $\phi = 0.25$ and 0.4, respectively.

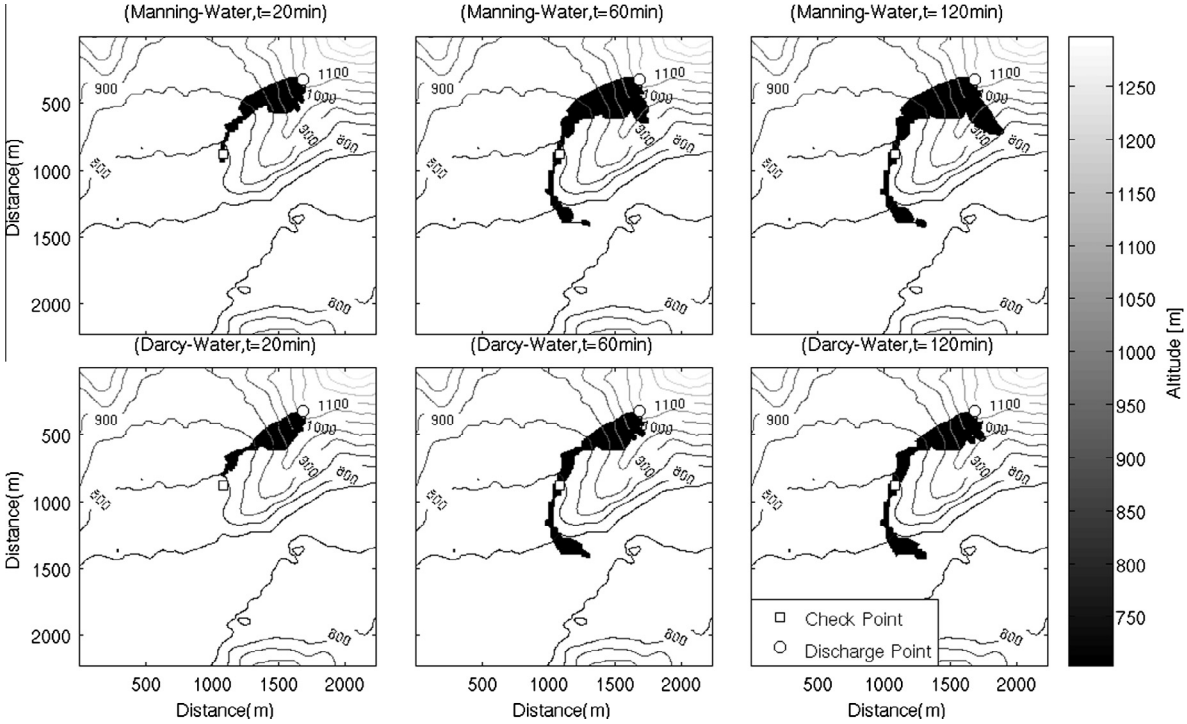

Fig. 5. Water run-out in the steep slope scenario for a 600 m^3/h discharge flow. The first and second rows show the simulation results using the Manning and Darcy coefficient formulations, respectively.

overestimation is therefore a consequence of both the smooth wall turbulent and laminar regimes, where the friction factor becomes a decreasing function of the local Reynolds number.

On the other hand, the second important driver in the problem is the relative importance of the frictional and inertial terms in (22b) and (22c), an aspect that is strongly controlled by the local slope conditions. In particular, the bottom shear stress depends directly on the Reynolds number; for higher values of Re_k and Re_B the values of the Darcy coefficient become weakly dependent of the rheology and strongly dependent on the flow characteristics (specifically on the ratio H/k_s). Higher values of Reynolds numbers may be obtained in high slope scenarios, where rheology has only a

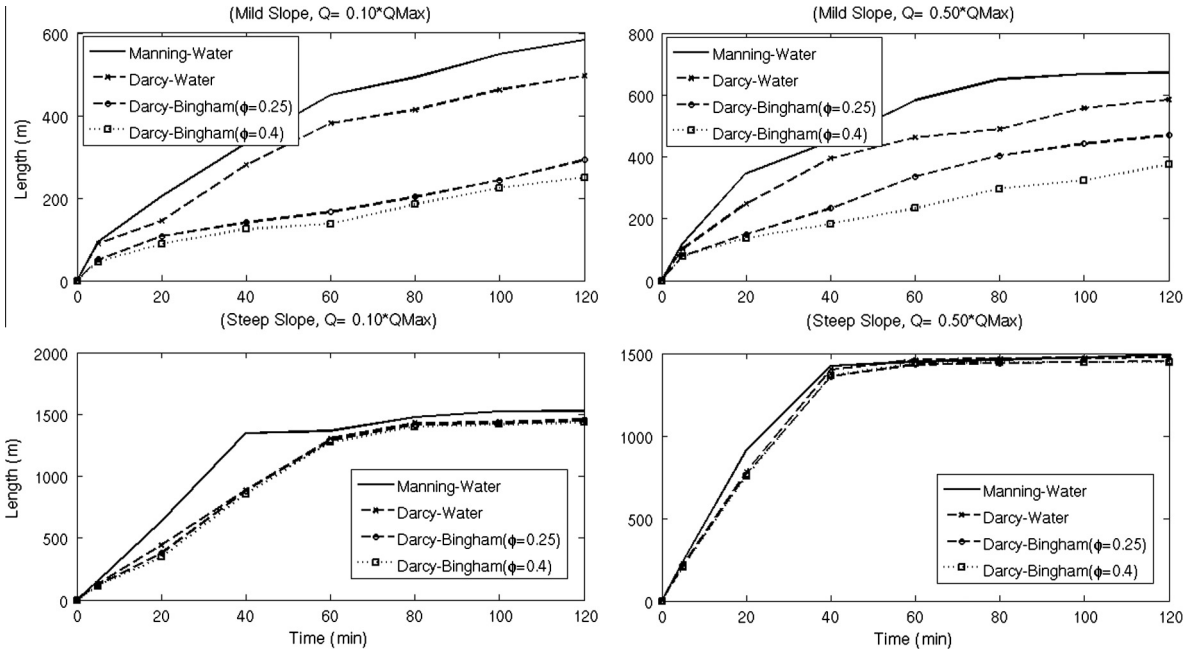

Fig. 6. Flow run-out lengths along the main spreading axis for different cases.

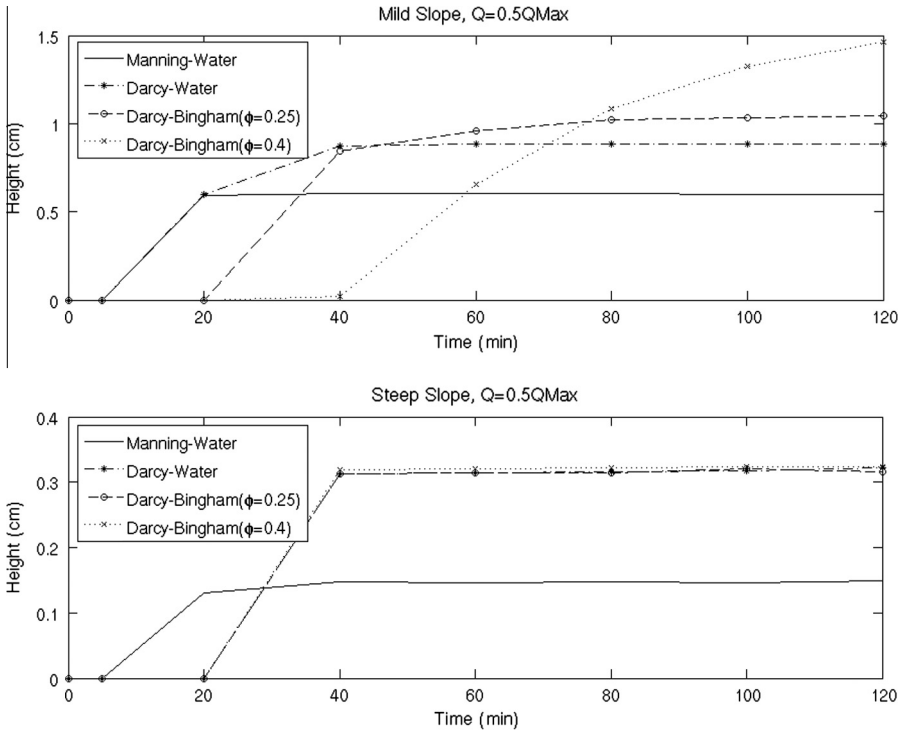

Fig. 7. Flow heights at selected checkpoints for each topography, as shown in Figs. 2–5. The discharge flow is 600 m^3/h.

second-order role. In a steep slope scenario, the differences between using water and slurries are slight, as seen on Fig. 5. In spite there are no further results presented using the Darcy coefficient formulation, due to almost identical results obtained when comparing flow run-outs for them at steep slope scenarios, there are not great differences in the progression of the spread, as shown in Fig. 6. The latter observation is also supported by the results in Fig. 7 for the steep slope, where the arrival of the flow at the checkpoint is at the same time for all Darcy cases and it differs only from the arrival of the Manning case.

Eqs. (22a)–(22c) give an indication of the small differences between the different steep slope cases analysed. The dimensionless form of the Saint–Venant show the product of order 1 quantities and the dimensionless numbers Fr_i, L and ε_i, as defined in (23)–(25). The characteristic scales are the same for each topographic scenario and the only variation is the formulation used to model the shear stress and the corresponding rheology. As the dimensionless numbers are fixed, the only possible origin of the differences in results corresponds to the Darcy friction coefficient, which depends directly on the Reynolds number. When high

values of the latter are present, f becomes Reynolds number-independent. This is so in the steep slope scenario where it is found that the gravity force driving the flow is mainly counterbalanced by the roughness-driven frictional mechanism, thus deeming viscosity only a second order effect. This may be seen in the frictional term, consisting of the right hand side of (22b) and (22c), which is proportional to $Fr^2 f$. The highest possible values of this term occur at laminar flow, i.e., for $f \sim 1/Re_B$. In the steep slope cases, the values of Fr^2/Re_B have a modest variation – between 0.0168 and 0.017 –, regardless the solids concentration, an indication of the weak importance of the latter in this regime. On the other hand, for the same instances, Fr^2 is on the order of 3, thus suggesting that for high slopes the inertial term of the momentum equation dominates over the effect of the slurry viscosity in a wide range of solids concentrations. In contrast, this is not true when the spreading occurs over mild slopes, where different results are found for the various bottom shear stress formulations, Manning or Darcy, and solids concentrations In particular, the yield stress and plastic viscosity strongly control the final spreading of the flow. Figs. 2–4 depict this situation: as intuitively expected, higher concentrations imply higher viscous stresses and thus a different point of balance with inertia and gravity. As the yield stress grows, the flow tends to stop sooner as the fluid does not allow deformation at scales below about the one-dimensional static balance condition $\tau_y(\phi)/(\rho_m(\phi)gH\sin(\theta))$, where θ is the local angle of inclination in the direction of the flow. On the other hand, increasing the plastic viscosity may cause a significant decrease in the flow velocity: assuming a uniform flow and low to moderate Reynolds numbers, the mean flow velocity is roughly proportional to $\eta^{-1/(2/a-1)}$, where a takes values between about 0.2 when hydrodynamically smooth wall turbulence occurs (Darby, 2001) and 1, when the flow is laminar. On the other hand, variations of the concentration in the fluid are evidenced with the flow height development, where a tendency to a stable or quasi-permanent height is observed. This is shown in Fig. 7, where it is also shown that higher viscosities require greater stabilisation times. In contrast to the steep slope scenario, for the mild slope computations, the dimensionless number Fr^2/Re_B have strong variations among the different concentrations. This confirms not only the differences in the spreading all along the simulation but also the importance of the rheology as an energy-balancing element in mild slopes.

Figs. 6 and 7 imply a challenge to emergency response planning, and give a strong indication on the need to support results with proper modelling. Following the Manning approach, remediation operations would need to start virtually immediately. However, considering that the Manning approach is a less accurate formulation for slurry flows, conclusions should be obtained from the friction factor approach instead. In the examples presented in this article, the results obtained using the Darcy friction factor to compute the bottom shear stress are similar, showing differences in the shape of the spill, and in the length at a given time, for the topography with lower slope. Given the present results, for the example cases presented, with a check point at 159 and 815 m to their respective leak scenario, the response team should not take more than 20 min to react or realize a rupture has happened and, on the other hand, efforts to contain the should not be delayed over an hour since the beginning of the leak.

From present computations, the available topographic data obtained from digital elevation models (DEM) is sufficient as a first approach for simulations, but further campaigns to obtain a detailed georeferred elevation data are necessary to exploit all the benefits of a numerical model of the characteristics presented in this paper. In particular, such campaigns would be extremely useful to gain insights on the flow at microscale, where most likely channels with flow heights potentially on the dozens of centimetres would be prone to form. Nonetheless, present results are yet useful to predict the rate of spreading of the spills on the grid scale (in this case, close to 5×5 m^2).

7. Conclusions

In the present paper, a systematic CFD approach has been proposed to analyse the flow resulting from a pipeline leak on a natural topography. The differences between the bed shear stress formulations are remarkable. Whereas there is no doubt of the general value and simplicity of the Manning approach for water flows, in light of present results, the pertinence of such approach depends on the topographic conditions and of the fluid being transported. In the particular case of middle-to-high volume fractions of ore concentrates, it has been shown that this global friction parameterisation should be replaced by a flow-dependent approach, as it has been used herein *via* the Darcy formulation, at a modest computational cost. Quantitatively, the use of a single Manning coefficient yields a systematic overestimation of final spill lengths and mean flow velocities, whereas underestimations of flow height calculations are also observed.

The possibility of introducing parameters characterizing the rheology of the fluid adds generality to the type of non-Newtonian fluid spill that could be potentially modelled, thus allowing to the consideration of a relatively large number of scenarios in risk analysis studies. Further extensions, including the potential to implement a time-dependent discharge curve – a useful feature for real pipeline leak simulations accounting for confined volumes and nearest valve locations – or the inclusion of other rheological models (Bird et al., 1983) is still a challenge towards the goal of achieving a more general and accurate description.

Acknowledgements

The authors gratefully acknowledge support from the Department of Civil Engineering of University of Chile and the Chilean National Commission for Scientific and Technological Research, CONICYT, through Fondecyt Project No. 11110201 and 1130910. The first author would also like to thank the scholarship for Master Program CONICYT-PFCHA/Magíster Nacional/2013 folio 221320183.

The authors would like to thank Judith Eeckman whose collaboration in the understanding of GEOCLAW and FORTRAN language was an important part of this work.

References

Abulnaga, B.E., 2002. Slurry Systems Handbook. McGraw-Hill, New York.
Aldrighetti, E., Zanolli, P., 2005. A high resolution scheme for flows in open channels with arbitrary cross-section. Int. J. Numer. Meth. Fluids 47 (8–9), 817–824.
Berger, M.J., George, D.L., Le Veque R.J., Mandli, K.T., 2011. The GEOCLAW software for depth-averaged flows with adaptive refinement. Adv. Water Res. 34 (9), 1195–1206.
Bird, R.B., Dai, G.C., Yarusso, B.J., 1983. The rheology and flow of viscoplastic materials. Rev. Chem. Eng. 1 (1), 1–70.
Biscarini, C., Francesco, S.D., Manciola, P., 2010. CFD modelling approach for dam break flow studies. Hydrol. Earth Syst. Sci. 14 (4), 705–718.
Brufau, P., Garcia-Navarro, P., 2000. Two-dimensional dam break flow simulation. Int. J. Numer. Meth. Fluids 33 (1), 35–57.
Buckingham, E., 1921. On plastic flow through capillary tubes. In Proc. Am. Soc. Test. Mater. 21, 1154–1156.
Chhabra, R.P., Richardson, J.F., 2008. Non-Newtonian Flow and Applied Rheology: Engineering Applications, second ed. Butterworth-Heinemann.
Darby, R., 2001. Chemical Engineering Fluid Dynamics. Marcel Dekker Inc., New York.
Eshtiaghi, N., Markis, F., Slatter, P., 2012. The laminar/turbulent transition in a sludge pipeline. Water Sci. Technol. 65 (4), 697–702.
Faddick, R.R., 1985. Hydrotransport of concentrated slurries and tailings. Lecture notes of the course dictated at the School of Engineering, Catholic University of Chile, sponsored by the United Nations.
George, D.L., 2008. Augmented Riemann solvers for the shallow water equations over variable topography with steady states and inundation. J. Comput. Phys. 227, 3089–3113.

George, D.L., Le Veque, R.J., 2006. Finite volume methods and adaptive refinement for global tsunami propagation and local inundation. Sci. Tsunami Hazard. 32 (5), 319.
George, D.L., Le Veque, R.J., 2008. High-resolution finite volume methods for the shallow water equations with bathymetry and dry states. Adv. Numer. Model Simulating Tsunami Waves Runup 10, 43–73.
Godunov, S.K., 1959. A difference method for numerical calculation of discontinuous solutions of the equations of hydrodynamics. Matematicheskii Sbornik 89 (3), 271–306.
Heymann, L., Peukert, S., Aksel, N., 2002. On the solid–liquid transition of concentrated suspensions in transient shear flow. Rheol. Acta 41 (4), 307–315.
Ihle, C.F., Tamburrino, A., 2012a. A note on the Buckingham equation. Can. J. Chem. Eng. 90, 944–945.
Ihle, C.F., Tamburrino, A., 2012b. Uncertainties in key transport variable in homogenous slurry flows in pipelines. Miner. Eng. 32, 54–59.
Ihle, C.F., 2013. A cost perspective for long distance ore pipeline water and energy utilization. Part I: Optimal base values. Int. J. Miner. Process. 122, 1–12.
Jia, Y., Wang, S.S., 1999. Numerical model for channel flow and morphological change studies. J. Hydraulic Eng. 125 (9), 924–933.
Keulegan, G.H., 1938. Laws of Turbulent Flow in Open channels. J. Res. National Bureau Standards, paper RP 1151 21, 707–741.
Limerinos, J.T., 1970. Determination of the manning coefficient from measured bed roughness in natural channels. US Government Printing Office, p. 53.
Mewis, J., Wagner, N.J., 2011. Colloidal Suspension Rheology. Cambridge University Press.
Minas, G., 2010. Vazamento de minério de ferro atinge rio de Minas Gerais', O Globo. URL: http://extra.globo.com/noticias/brasil/vazamento-de-minerio-de-ferro-atinge-rio-de-minas-gerais-160631.html. In Portuguese.
Nikuradse, J., 1950. Strömungsgesetse in rauhen Rohren. VDI-Forschungsheeft 361. Beilage zu Forschung auf dem Gebiete des Ingenieurwesens, Ausgabe B Band 4. Also as Laws of flow in rough pipes, NACA, Technical, Memorandum 1292.
Skelland, A.H.P., 1967. Non-Newtonian flow and Heat Transfer. John Wiley & Sons.
Toro, E.F., 1997. Riemann Solvers and Numerical Methods for Fluid Dynamics: a Practical Introduction. Springer-Verlag, Berlin Heidelberg.
Thomas, A.D., Wilson, K.C., 1987. New analysis of non-newtonian turbulent flow – Yield-power-law fluids. Can. J. Chem. Eng. 65 (2), 335–338.
Torrance, B.M., 1963. Friction factors for turbulent non-Newtonian flow in circular pipes. SA Mech. Eng. 13, 89–91.
Wasp, E.J., Kenny, J.P., Gandhi, R.L., 1977. Solid–liquid flow slurry pipeline transportation. Trans Tech Publications.
White, F.M., 2003. Fluid Mechanics, fifth. ed. McGraw-Hill Book Company, Boston.
Xia, B., Sun, D.W., 2002. Applications of computational fluid dynamics (CFD) in the food industry: a review. Comput. Electron. Agricult. 34 (1), 5–24.